Giantin is required for intracellular N-terminal processing of type I procollagen

Nicola L. Stevenson[1], Dylan, J. M. Bergen[2, 3], Chrissy L. Hammond[2], and David J. Stephens[1]*

* Corresponding author (david.stephens@bristol.ac.uk)

[1]Cell Biology Laboratories, School of Biochemistry, Faculty of Life Sciences, University of Bristol, Biomedical Sciences Building, University Walk, Bristol BS8 1TD, UK.

[2]School of Physiology, Pharmacology and Neuroscience, Faculty of Life Sciences, University of Bristol, Biomedical Sciences Building, University Walk, Bristol BS8 1TD, UK

[3]Musculoskeletal Research Unit, Translational Health Sciences, Bristol Medical School, Faculty of Health Sciences, University of Bristol, Southmead Hospital, Bristol, BS10 5NB, UK.

Condensed title: Giantin-dependent procollagen processing

Abstract

Knockout of the golgin giantin leads to skeletal and craniofacial defects driven by poorly studied changes in glycosylation and extracellular matrix deposition. Here, we sought to determine how giantin impacts the production of healthy bone tissue by focussing on the main protein component of the osteoid, type I collagen. Giantin mutant zebrafish accumulate multiple spontaneous fractures in their caudal fin, suggesting their bones may be more brittle. Inducing new experimental fractures revealed defects in the mineralisation of newly deposited collagen as well as diminished procollagen reporter expression in mutant fish. Analysis of giantin knockout cells expressing a GFP-tagged procollagen showed that procollagen trafficking is independent of giantin. However, our data show that intracellular N-propeptide processing of pro-α1(I) is defective in the absence of giantin. These data demonstrate a conserved role for giantin in collagen biosynthesis and extracellular matrix assembly. Our work also provides evidence of a giantin-dependent pathway for intracellular procollagen processing.

Introduction

The golgins are a family of coiled-coil domain proteins that extend out from the surface of the Golgi apparatus to tether transport vesicles and other Golgi membranes (Munro, 2011). The largest member of this family, giantin, is a tail-anchored membrane protein with a predicted 37 cytosolic coiled-coil domains (Linstedt and Hauri, 1993; Seelig et al., 1994). These structural features are key attributes for a membrane tether, however, to date no tethering function for giantin has been identified. Indeed, giantin loss does not block anterograde transport (Lan et al., 2016; Stevenson et al., 2017) and may in fact accelerate it (Koreishi et al., 2013). Most studies also agree that giantin is not essential to maintain Golgi morphology (Koreishi et al., 2013; Lan et al., 2016; Puthenveedu and Linstedt, 2001; Stevenson et al., 2017), although it may inhibit lateral tethering between cisternae (Satoh et al., 2019; Stevenson et al., 2017). Discrepancies between these studies are likely due to variation in levels of depletion (Stevenson et al., 2017), in genetic compensation (Stevenson et al., 2017), and/or functional redundancy with other golgins (Wong and Munro, 2014).

The most consistent observation from published work is that giantin is required to regulate glycosylation (Kikukawa et al., 1990; Koreishi et al., 2013; Lan et al., 2016; Petrosyan et al., 2014; Stevenson et al., 2017) and extracellular matrix (ECM) formation (Katayama et al., 2018; Kikukawa and Suzuki, 1992; Lan et al., 2016). Highly selective defects in *O*-glycosylation have been reported following knockout (KO) of the *GOLGB1* gene encoding giantin in cells (Stevenson et al., 2017), zebrafish (Stevenson et al., 2017), and mice (Lan et al., 2016). Enzyme distribution (Petrosyan et al., 2014) and surface glycosylation patterns (Koreishi et al., 2013) are more generally affected following siRNA depletion. The secretion of ECM proteoglycans and collagen can also be affected (Katayama et al., 2018; Kikukawa et al., 1990). The primary phenotype shared by all *GOLGB1* KO animal models is the abnormal development of craniofacial structures, whilst species specific phenotypes include short limbs in rats (Katayama et al., 2011) and ectopic mineralisation of soft tissues in zebrafish (Stevenson et al., 2017). Giantin is therefore important for skeletal development and defects in ECM quality likely underly all these phenotypes.

In light of these observations, we hypothesised that giantin may regulate secretion of the primary protein component of skeletal ECM, fibrillar type I collagen. In mammals, this is predominantly built from heterotrimeric molecules composed of two pro-α1(I) chains (encoded by the *COL1A1* gene) and one pro-α2(I) chain (encoded by *COL1A2*) chain. Structurally, each chain is made up of a helical domain, composed of Gly-X-Y repeats, flanked by globular N- and C-propeptide domains (Canty and Kadler, 2005). These chains are co-translationally translocated into the endoplasmic reticulum (ER) lumen where they are post-translationally modified prior to folding into a right-handed triple helical molecule. Trimeric procollagen is exported from the ER and transits the Golgi before being secreted from the cell and assembled into fibrils in the ECM (Canty and Kadler, 2005; Canty et al., 2004).

Prior to fibrillogenesis, the N- and C-propeptide domains of procollagen are cleaved to promote correct alignment and polymerisation. Removal of the C-propeptide is particularly critical as this induces self-assembly of collagen into fibrils (Hulmes et al., 1989; Kadler et al., 1987; Kadler et al., 1990; Miyahara et al., 1984; Miyahara et al., 1982). Retention of the N-propeptide on the other hand does not preclude fibril assembly but can affect fibril morphology (Bornstein et al., 2002; Hulmes et al., 1989; Romanic et al., 1992). C- terminal processing is carried out by BMP-1/tolloid-like family metalloproteinases (Kessler et al., 1996) while ADAMTS2, -3 and -14 cleave the N-propeptide (Bekhouche and Colige, 2015; Colige et al., 1997; Colige et al., 2002; Fernandes et al., 2001). Meprin α and meprin β have also been implicated in procollagen processing (Broder et al., 2013).

In this study, by using a combination of fin fracture assays in *golgb1* mutant zebrafish and biochemical assays in giantin KO cells, we demonstrate that giantin function is required to facilitate normal fracture repair and for intracellular N-terminal processing of type I procollagen.

Results

Homozygous golgb1 mutant fish have a higher incidence of fracture

To begin our investigation into the role of giantin in the deposition of skeletal ECM we first examined our previously published homozygous (HOM) *golgb1*$^{X3078/X3078}$ mutant zebrafish line for bone defects (Stevenson et al., 2017). Focussing on the experimentally tractable caudal fin (Bergen et al., 2019), we observed an unusually high number of naturally occurring fractures in the hemirays of homozygous (HOM) individuals compared to wild type (WT) and heterozygote (HET) siblings. This was seen both in terms of the number of injured fish and the number of fractures per individual. Indeed at 7 months old, 76% of HOM fish had acquired at least one fracture compared to just 33% of WT and 27% of HET fish (Figure 1A). The mean number of fractures per individual was 0.4 for WT and HETs and 1.8 for mutants. Interestingly, four or more fractures were detected in 12% of *golgb1*$^{X3078/X3078}$ mutants. This was never seen in WT or HET siblings. These were often in the proximal half of the fin and occurred either consecutively along one ray or adjacent to each other in parallel rays (Figure 1B). There was also one HOM individual carrying fractures that had fused together, indicating aberrant fracture repair with excessive calcification (Figure 1B).

golgb1 mutant fish show mineralisation defects during fracture repair

To look at fractures more closely, fractures were experimentally induced in caudal fin hemirays of mutant and WT fish as has been previously described (Geurtzen et al., 2014; Tomecka et al., 2019). Injured fish were stained with calcein at different timepoints to monitor calcification of newly formed bone matrix in the callus. Calcein labelling was first visible in WT fish four days post injury (dpi) whereas labelling was already apparent at the fracture site in HOM fish at 2 dpi (Figure 1C-D). In both cases labelling intensity continued to increase over time, peaking at 10 dpi. Calcein fluorescence was substantially greater in the fractures of HOM fish throughout the assay. This is most evident at 10 dpi when it was approximately 400% brighter in the mutants. Levels of calcein-accessible calcium are therefore elevated in the fractures of *golgb1*$^{X3078/X3078}$ fish. This shows that premature and enhanced calcification occurs in the mutant fish.

Expression of the *col1a1* gene is reduced in *golgb1* mutant fractures

Mineralisation is dependent on the correct spatio-temporal deposition of a collagen matrix to ensure the right amount of calcification occurs at the right time (Michigami, 2019). We therefore looked at type I collagen expression in the repairing fractures. We crossed *golgb1*$^{X3078/X3078}$ fish with a *col1a1a:GFP* promoter reporter line and performed the same fracture experiments as above but without the calcein stain. Expression of *col1a1a:GFP* at the fracture site relative to healthy bone was highest at 4 dpi in both HET and HOM fractures (Figure 1E-F). Expression returned to normal levels by 14 dpi. Interestingly, *col1a1a:GFP* expression was lower in the mutant fractures compared to HETs at both 4 and 7 dpi when promoter activity was at its peak. This agrees with our previously published RNAseq data which shows a reduction in *COL1A1* mRNA in *GOLGB1* KO hTERT-RPE1 cells relative to WT (Stevenson et al., 2017). No obvious difference in callous width or alizarin red staining was observed (Supplemental Figure 1).

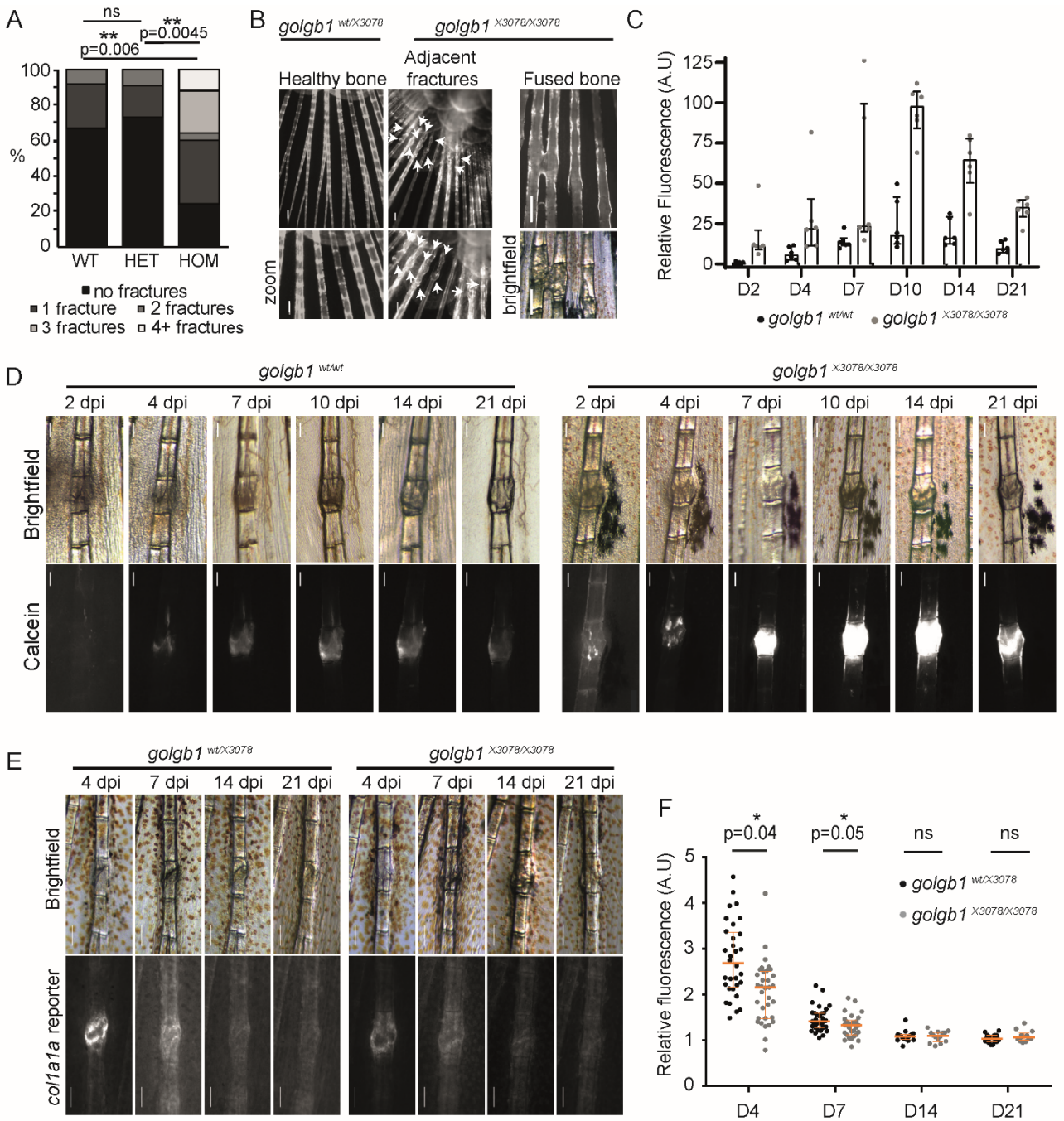

Figure 1. Fracture defects in *golgb1* mutant zebrafish. A. Quantification of the number of fractures naturally found in the caudal fin of WT and *golgb1*^{X3078} heterozygous and homozygous mutant fish at 7 months old. Data show % of fish with x number of fractures (WT=12 fish, HET=11 fish, HOM=25 fish from 2 independent crosses). **B**. Fluorescence images of naturally occurring caudal fin defects in *golgb1*$^{X3078/X3078}$ fish stained with alizarin red. White arrows indicate fractures. Scale bar 200 µm. **C-D.** Quantification (C) and representative brightfield and fluorescent images (D) of experimentally induced fractures in *golgb1*$^{wt/wt}$ *and golgb1*$^{X3078/X3078}$ caudal fins on different days post-injury (dpi). Bone was stained with calcein at each timepoint prior to imaging. (C) Calcein intensity in fractures was measured relative to that of healthy adjacent bones. Lower exposure images than those in D were used for quantification to avoid saturation. Each dot represents one fracture. Bars show median and interquartile range (2 fish per line quantified, each with 3 fractures). (D) Proximal end of bone is at the top of image. Scale bar 200 µm. **E.** Representative brightfield and fluorescent images of experimentally induced fractures in the caudal fin of *golgb1*$^{wt/X3078}$ *and golgb1*$^{X3078/X3078}$ fish expressing a *col1a1a:GFP* promoter reporter at different timepoints. Proximal end of bone is at the top of image. Scale bar 200 µm. **F.** Quantification of *col1a1a:GFP* signal at the fracture site relative to an adjacent healthy bone. Each dot represents one fracture. Orange bars indicate median and interquartile range. At timepoints 4 and 7 d.p.f eleven fish per line were quantified. At timepoints 14 and 21 d.p.f n= 6 HETs and n=4 HOM fish quantified. All data was collected in a single experiment. All p values were calculated with the Mann-Whitney U test comparing the means for each fish, 3 fractures per fish.

128 **Expression and secretion of type I collagen is elevated in giantin KO cells**

129 To better understand the matrix defects observed above, we turned to our previously published *GOLGB1*
130 KO hTERT-RPE1 cell line to study collagen secretion in a more tractable system (Stevenson et al., 2017). Our
131 previously published RNAseq data shows that gene expression of *COL1A1* is reduced in giantin KO cells
132 (Stevenson et al., 2017). In contrast, immunoblot analysis shows that KO cells contain higher levels of pro-
133 α1(I) protein relative to WT cells (Figure 2A-B). While statistical testing of pooled data does not reveal a
134 detectable difference here, comparison of individual experiments (colour-coded in Figure 2B) shows a
135 consistent increase of pro-α1(I). Interestingly, higher procollagen levels are not due to protein retention
136 since KO cells also secrete similar or higher amounts of pro-α1(I) compared to WT cells, both in absolute
137 terms and relative to the intracellular pool (Figure 2C-D). There is also no evidence of collagen over-
138 modification or ER dilation (Stevenson et al., 2017) as would be expected if the collagen were retained
139 (Ishida et al., 2006). Immunofluorescence labelling of pro-α1(I) in non-permeabilised WT and KO cells
140 verified that this excess of secreted collagen is incorporated into the extracellular matrix (Figure 2E).

141 To determine whether the organisation of the matrix produced by KO cells is altered compared to WT, we
142 stripped the cell layer from 7-day confluent cultures and imaged the cell derived matrix (CDM) both by
143 scanning election microscopy (Figure 2F) and by confocal microscopy after immunolabelling for pro-α1(I)
144 (Figure 2G). In each case, the giantin KO CDM often appeared to contain thicker fibres that were more
145 intensely labelled for pro-α1(I).

146

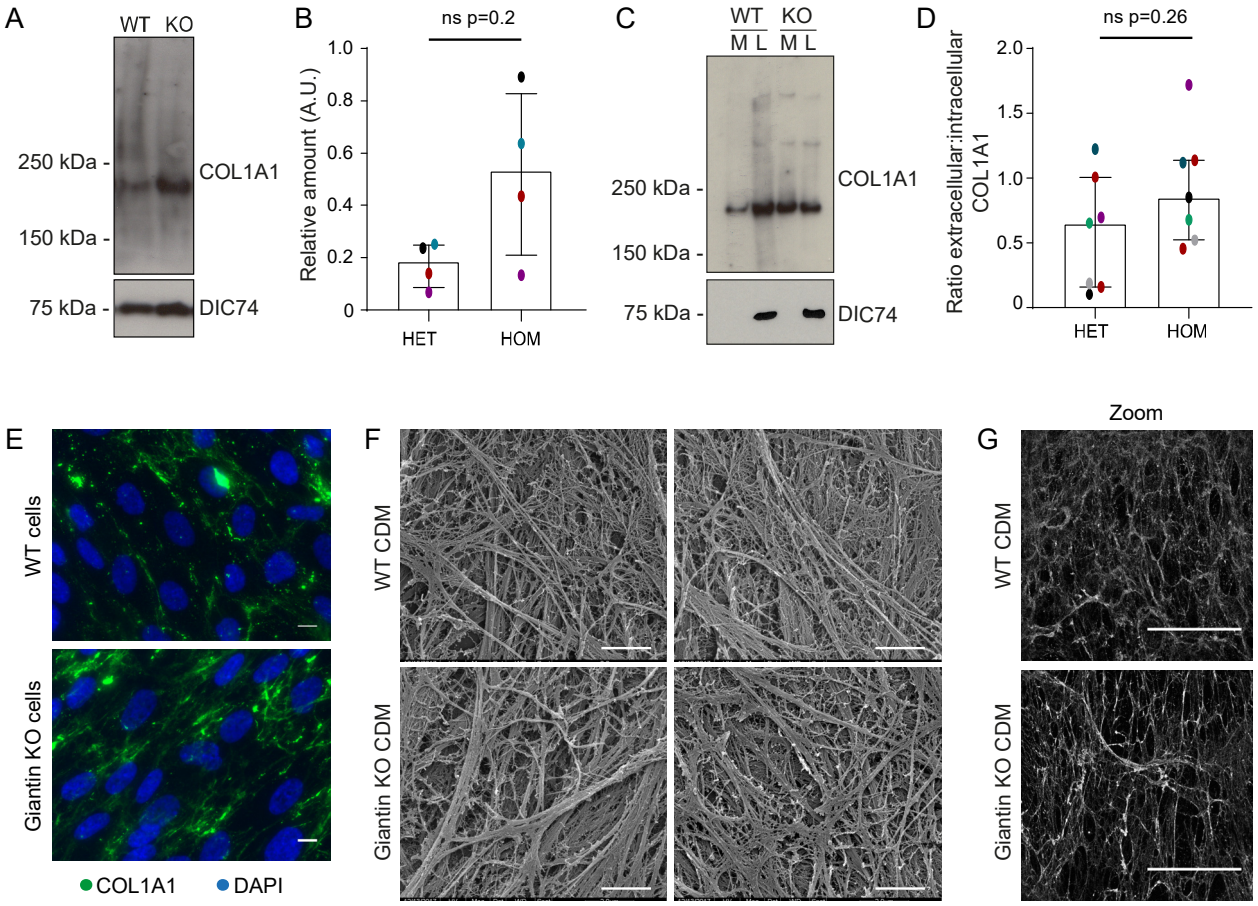

Figure 2. pro-α1(I) is more abundant in giantin KO cells. **A**. Western blot of pro-α1(I) (COL1A1) and dynein intermediate chain (DIC74, housekeeping) in cell lysates taken from WT and giantin KO cells. **B.** Densitometry of the semi-quantitative ECL western blots represented in (A). Dots show individual replicates and each independent experiment is colour-coded between cell lines. Bars depict median intensity of pro-α1(I) (COL1A1) normalised against DIC74 (n=4 biological replicates). Error bars = interquartile range. Statistical test Mann-Whitney **C.** Western blot of media (M) and cell lysate (L) fractions taken from WT and giantin KO cell cultures after 16 h incubation with serum free medium plus 50 µg/µl ascorbate. **D.** Ratio of extracellular vs intracellular levels of collagen as measured from secretion assays represented in (C). pro-α1(I) (COL1A1) levels measured by densitometry from semi-quantitative ECL blots and normalised against DIC74 before calculating ratios. Dots show individual replicates and each independent experiment is colour-coded between cell lines. Bars depicts median and interquartile range (n=7 biological replicates). Statistical test Mann-Whitney **E**. Maximum projections of widefield image stacks showing PFA fixed, unpermeabilised cells immunolabelled for endogenous pro-α1(I) (COL1A1, green). Nuclei are stained with DAPI (blue). Scale bars 10 µm. **F-G**. The cell derived matrix produced by WT and giantin KO cells imaged as (A) scanning electron micrograms, and (B) confocal z stacks of antibody labelled pro-α1(I) presented as maximum projections. Scale bars 2 µm (A) and 100 µm (B).

164 **Procollagen trafficking through the early secretory pathway is unaffected by loss of giantin**

165 We next tested whether altered procollagen synthesis and deposition is the result of changes to
166 procollagen trafficking through the secretory pathway. To this end, we generated WT and giantin KO cell
167 lines stably expressing low levels of proSBP-GFP-COL1A1 (GFP-COL1A1, (McCaughey et al., 2019)). This
168 construct encodes pro-α1(I) with a GFP and SBP tag inserted upstream of the N-propeptide cleavage site
169 (Figure 3A). The SBP tag allows controllable bulk release of the procollagen from the ER using the Retention
170 Using Selective Hooks assay (RUSH, (Boncompain et al., 2012)). This assay relies on co-expression of a KDEL-
171 streptavidin hook to bind the SBP and anchor the GFP-COL1A1 in the ER. The experimental addition of
172 biotin then displaces the SBP, releasing the procollagen. The hook is co-expressed from a bicistronic vector
173 with mCherry-sialyltransferase (mCh-ST) which labels the Golgi.

174 In WT cells, the GFP-COL1A1 first accumulates around the mCh-ST positive Golgi compartment upon
175 release (Figure 3B, Supplemental Movie 1). Fixation at this timepoint followed by immunolabelling of Golgi
176 markers confirmed that this predominantly represents the GFP-COL1A1 entering the *cis*-Golgi (Figure 3E).
177 Shortly after *cis*-Golgi filling, the GFP-COL1A1 progresses through the Golgi into the mCh-ST-positive
178 cisternae before leaving the Golgi in tubular vesicular carriers (Figure 3B-C arrow). This "short loop"
179 pathway from the ER to cis-Golgi in the absence of discernible carriers has been described previously
180 (McCaughey et al., 2019). Crucially here, we found that GFP-collagen also traverses this pathway in the
181 giantin KO cells (Figure 3C, Supplemental movie 2).

182 To measure the kinetics of ER-to-*cis*-Golgi transport we quantified the time between biotin addition and the
183 appearance of the GFP-COL1A1 in the *cis*-Golgi. Trafficking rates were equivalent in both cell lines (Figure
184 3D). We therefore conclude that the collagen phenotypes seen in giantin KO cells are not due to the use of
185 an alternative trafficking route or faster kinetics.

186

187

188

189

190

191

192

193

194

195 *Over page:*

196 **Figure 3. ER-Golgi trafficking of pro-α1(I) is unperturbed in giantin KO cells**. **A** Schematic of the pro-SBP-GFP-COL1A1
197 construct used in this study. SS = signal peptide SBP = streptavidin binding protein. **B-C**. Single plane confocal stills
198 taken from live imaging movies of a (A) WT and (B) giantin KO cell stably expressing GFP-COL1A1 (green) and
199 transiently transfected with mCh-ST (magenta) and an ER RUSH hook. Frame times in the top left corner indicate the
200 time (minutes) post biotin addition which releases GFP-COL1A1 from the ER hook. Scale bars 10 µm on overview and 1
201 µm on zoom. White arrows indicate the appearance of peripheral GFP-COL1A1 punctate. Orange arrows indicate
202 emerging post-Golgi carriers. See also supplemental movies. **D.** Quantification of the time taken for GFP-COL1A1 to
203 first appear at the Golgi in movies represented in (A-B). Each dot represents one cell (16 WT cells and 13 giantin KO
204 cells) and movies were collected over 7 independent experiments. Bars represent median and interquartile range.
205 Results are not significant using a Mann-Whitney-U test. **E.** Maximum projections of confocal z stacks of WT and
206 giantin KO cells imaged live as in (A-B) and then fixed with PFA as soon as the GFP-COL1A1 appeared around the Golgi.
207 Cells were then immunolabelled for the Golgi marker GM130 (blue). Scale bars 10 µm.

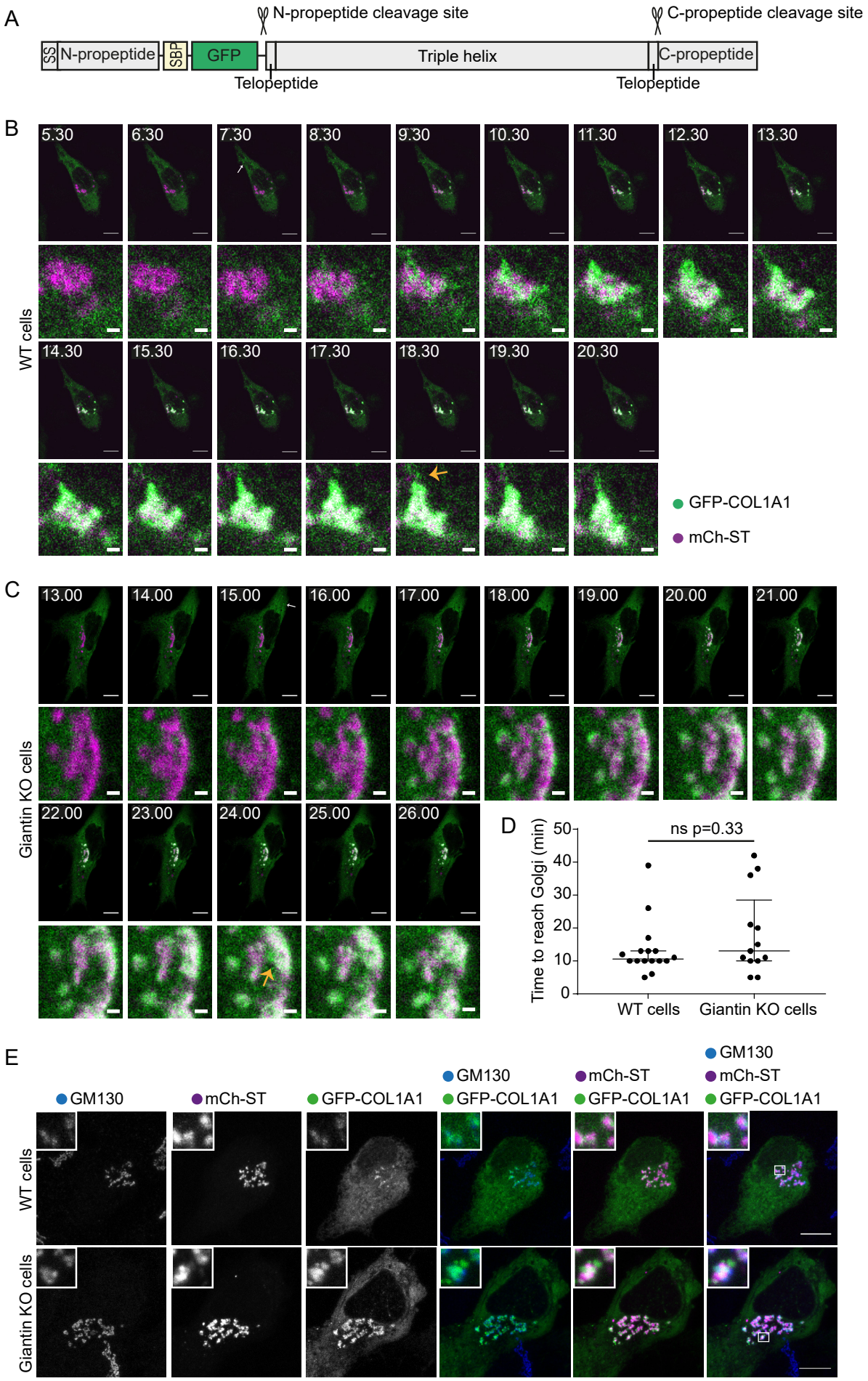
A
N-propeptide cleavage site
C-propeptide cleavage site
SS
N-propeptide
SBP
GFP
Triple helix
C-propeptide
Telopeptide
Telopeptide
B
WT cells
5.30
6.30
7.30
8.30
9.30
10.30
11.30
12.30
13.30
14.30
15.30
16.30
17.30
18.30
19.30
20.30
GFP-COL1A1
mCh-ST
C
Giantin KO cells
13.00
14.00
15.00
16.00
17.00
18.00
19.00
20.00
21.00
22.00
23.00
24.00
25.00
26.00
D
ns p=0.33
Time to reach Golgi (min)
50
40
30
20
10
0
WT cells
Giantin KO cells
E
GM130
mCh-ST
GFP-COL1A1
WT cells
Giantin KO cells

208

209 **Giantin KO cells exhibit defects in processing of type I procollagen**

210 During these experiments we observed that giantin KO cells stably expressing GFP-COL1A1 were often
211 surrounded by extracellular GFP-positive fibres. Immunofluorescence with a COL1A1 antibody identified
212 these as collagen fibrils, indicating that the GFP-tag is incorporated into the ECM (Figure 4A). No GFP-
213 COL1A1 positive fibrils could be detected in the matrix of WT cells despite an abundance of collagen and
214 the expression of GFP alone did not label the ECM.

215 In our reporter construct, GFP is inserted upstream of the N-propeptide cleavage site and should be
216 removed during processing (Figure 3A). The presence of GFP in the ECM therefore implies that either N-
217 propeptide processing is defective or that free N-propeptides are abnormally interacting with collagen
218 fibrils. To investigate this, we assayed secretion from these stable cell lines by immunoblotting. In both the
219 media and lysate fractions of WT cultures, a dominant GFP-positive band was discernible at ~60kDa, which
220 corresponds to the size of the tagged N-propeptide (Figure 4B). In KO cells, however, the dominant GFP-
221 positive band was detected at ~200kDa. This is consistent with the size of unprocessed, tagged procollagen.
222 No band was discernible at ~60kDa in the KO cells, even after enrichment by immunoprecipitation
223 (Supplemental Figure 2A) suggesting N-propeptide cleavage does not take place. These results were
224 supported by additional immunoblots detecting the SBP tag (Figure 4C). In this instance, full length
225 procollagen is also evident in WT cells, likely due to the higher affinity of the SBP antibody, but the N-
226 propeptide remains undetectable in the KO cells.

227 To verify our interpretation of these observations with respect to the N-propeptide, we performed
228 immunoblots using antibodies specifically targeting the N- and C-propeptide domains of pro-α1(I). C-
229 propeptide cleavage was comparable in WT and KO cells (Figure 4E) with bands of ~60 kDa and ~30 kDa
230 detected. However, an antibody against the N-propeptide detected a band of ~60kDa in WT cell lysates that
231 was again completely absent in the KO cultures (Figure 4F). This N-propeptide band was also detected in
232 the media of WT cells but only following enrichment by immunoprecipitation (Supplemental Figure 2A). It is
233 therefore present but in low quantities. Full length collagen protein levels were again higher in the KO cells
234 (Figure 4G).

235 We also used the N-propeptide-specific antibody (LF-39) to immunolabel the ECM of WT and KO cells.
236 Whilst this antibody failed to label the CDM of WT cells, it did label fibrils in the KO cell matrix where it
237 colocalised with the extracellular GFP signal (Figure 4H). Together these data indicate that the presence of
238 GFP in the collagen matrix of KO cells is due to a failure in N-propeptide cleavage. The above observations
239 are also consistent with N-propeptide cleavage taking place intracellularly in WT cells.

240 Secretion of unprocessed procollagen has been reported in the absence of Hsp47 (Ishida et al., 2006),
241 however, Hsp47 levels in the KO cells were normal, ruling this out as a cause (Supplemental Figure 2B-C).
242 We also hypothesised that the absence of N-propeptide in the KO cells could be due to its increased
243 degradation, but treatment of KO cells with proteasomal and lysosomal inhibitors did not render it
244 detectable (Supplemental Figure 2D). Interestingly, N-propeptide levels in the WT cells did change upon
245 treatment with these inhibitors, thus confirming the presence of an intracellular pool sensitive to these
246 pathways (Supplemental Figure 2D).

247

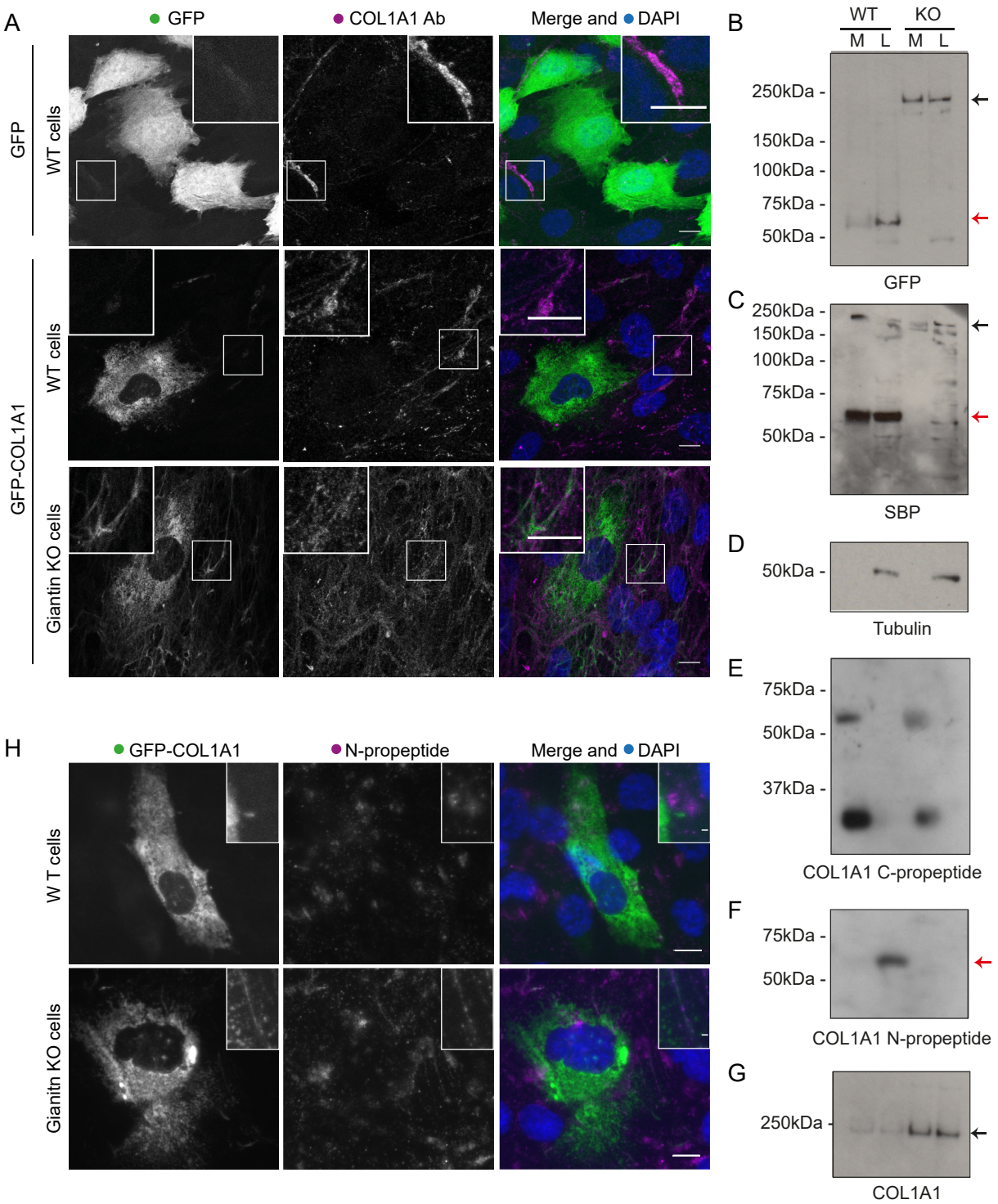

Figure 4. Procollagen processing is defective in giantin KO cells. A. Representative images of WT and giantin KO cell expressing GFP-COL1A1 or GFP alone as indicated and immunolabelled for pro-α1(I) (COL1A1, magenta). Nuclei are stained with DAPI (blue). Images are maximum intensity projections of widefield z-stacks. Scale bars 10 µm. **B-G.** Western blots of secretion assays showing the medium (M) and lysate (L) fractions of WT and giantin KO cell cultures immunoblotted for (B) GFP, (C) SBP, (D) Tubulin, (E) C-propeptide (LF41 antibody) (F) N-propeptide (LF39 antibody) and (G) pro-α1(I) (COL1A1). Black arrows indicate full length procollagen and red arrows highlight N-propeptide bands. **H.** Maximum intensity projection widefield z-stacks of WT and giantin KO cells stably expressing GFP-COL1A1 immunolabelled for the type I procollagen N-propeptide (LF39 antibody). Scale bars 10 µm.

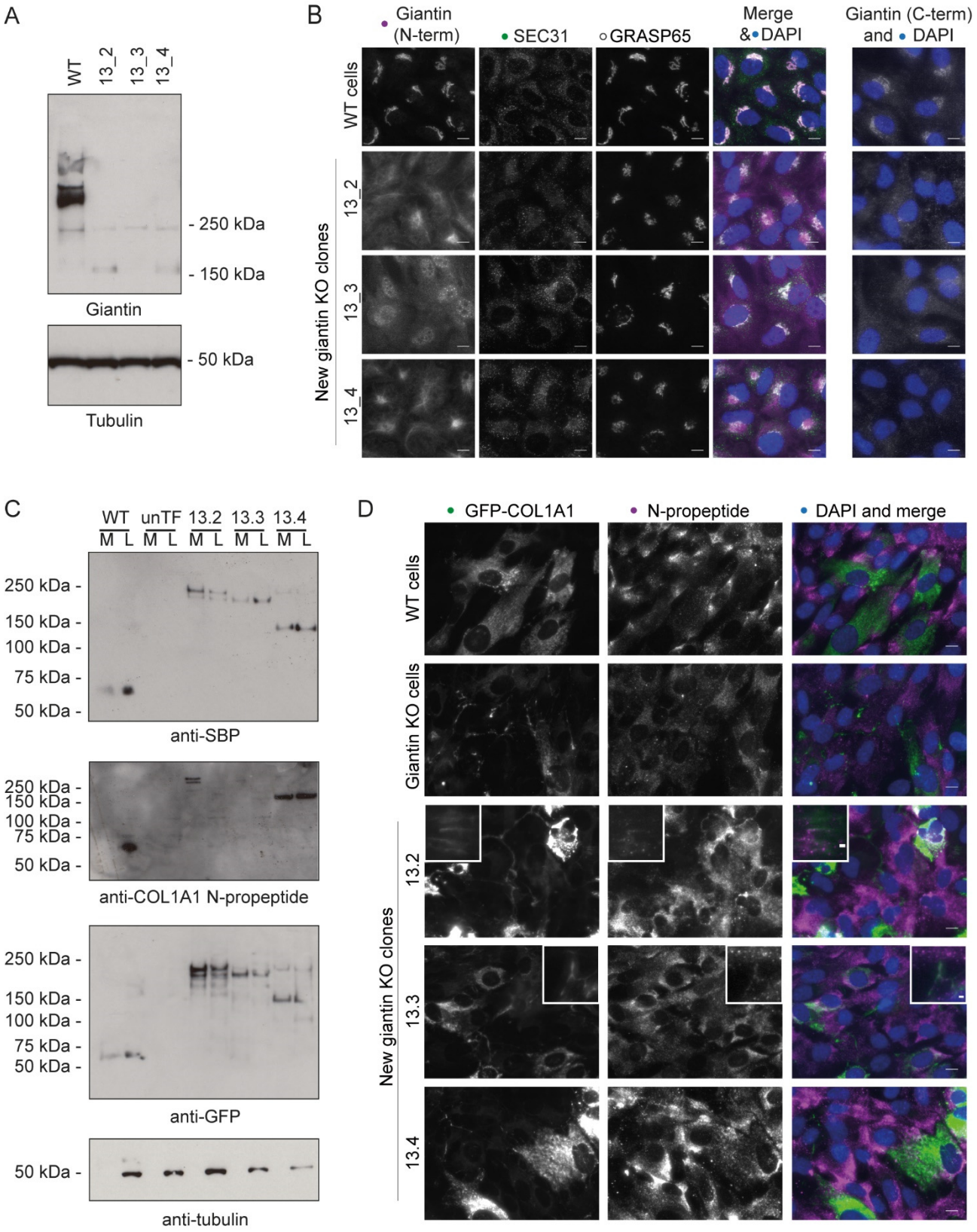

Figure 5. Validation of processing defects in other giantin mutant lines. A. Western blot of WT RPE1 and giantin exon 13 KO clone lysates probed for giantin (polyclonal against full length protein) and tubulin (housekeeping) **B.** WT and giantin KO RPE1 cell clones immunolabelled for the N- and C-terminus of giantin, ER exit sites (Sec31) and the Golgi (GRASP65) as indicated. Scale bar 10 µm. **C.** Western blots of secretion assays performed on WT and giantin KO clones stably expressing GFP-COL1A1 and untransfected giantin KO cells (unTF). Blots show the medium (M) and lysate (L) fractions of each cell population immunoblotted for GFP, SBP and type I procollagen N-propeptide as indicated. **D.** Maximum projection widefield images of GFP signal in giantin KO clones stably expressing GFP-COL1a1 and immunolabelled for pro-α1(I) N-propeptide (magenta). Scale bar 10 µm.

265 **N-terminal processing of type I procollagen is defective in other giantin KO lines**

266 Since the above data were derived from a single clone of *GOLGB1* KO cells, we generated new KO cell lines
267 in which to validate our findings. This time we targeted exon 13 of the *GOLGB1* gene (instead of exon 7)
268 and used the lentiCRISPRv2 system (Sanjana et al., 2014; Shalem et al., 2014) for transfection in order to
269 vary our approach. We obtained three clones with different indel mutations (Supplemental Figure 3).
270 Immunoblots with a giantin polyclonal antibody confirmed the loss of full-length protein, although hints of
271 a potential truncated form could be seen in low abundance (Figure 5A). Immunofluorescence staining with
272 antibodies targeting the N- and C- termini of giantin was unable to detect any protein (Figure 5B). As
273 previously described for the original knockout line (Stevenson et al., 2017), no gross changes in Golgi
274 morphology or ER exit site abundance were apparent following loss of giantin (Figure 5B).

275 Using the exon 13 mutant clones we derived new stable cell lines expressing GFP-COL1A1. We also made a
276 new WT GFP-COL1A1 stable line to be sure of the WT phenotype. As with our original clone, we were not
277 able to detect cleaved N-propeptide in either the media or lysate fractions from these new KO cell cultures
278 (Figure 5C). We did however note some variability in the molecular weight of the procollagen bands
279 detected between clones, perhaps suggesting additional processing defects or deficiencies in post-
280 translational modifications. Imaging of the new KO clones again also confirmed incorporation of the GFP-
281 tag and the N-propeptide into the extracellular collagen matrix in two of these lines (Figure 5D). The
282 phenotypes of the new WT stable cell lines also validated those of the original. Overall, these results
283 confirm that N-propeptide processing is defective in the absence of giantin.

284

285 ## Discussion

286 In this study we demonstrate for the first time that giantin is required for N-terminal, but not C-terminal,
287 processing of type I procollagen. In its absence, procollagen intermediates still bearing the N-propeptide
288 are secreted and incorporated into the ECM. Unlike the C-propeptide, retention of the N-propeptide does
289 not preclude fibril formation (Hulmes et al., 1989; Miyahara et al., 1984; Miyahara et al., 1982; Romanic et
290 al., 1992) and thus it is not surprising that a collagen fibrils are formed. We also found that free N-
291 propeptide is clearly detected in the cell layer of WT cells, implying it is cleaved inside the cell. Altogether,
292 these data indicate the presence of a giantin-dependent intracellular pathway for procollagen processing.

293 The most likely cause of the observed processing deficiency in KO cells is a defect in the expression,
294 trafficking, or processing of an N-proteinase. Although we have not yet identified any trafficking defects in
295 our giantin KO cells either generally (Stevenson et al., 2017) or specifically for procollagen, it is possible that
296 other cargoes such as processing enzymes will be affected. To date five enzymes have been implicated in
297 the N-terminal processing of type I procollagen - ADAMTS2, ADAMTS3, ADAMTS14 (Bekhouche and Colige,
298 2015; Colige et al., 1997; Colige et al., 2002; Fernandes et al., 2001), meprin-α and meprin-β (Broder et al.,
299 2013). Our previous RNAseq analysis of RPE1 cells (ArrayExpress E-MTAB-5618) failed to detect any
300 ADAMTS2 transcript, even in WT cells, however ADAMTS3 and -14 mRNA was present and interestingly
301 their expression was down-regulated following giantin KO (Stevenson et al., 2017). Unfortunately, our
302 attempts to further this line of enquiry have so far been unfruitful due to a lack of suitable reagents.

303 A second possible cause of defective processing is glycosylation deficiency. Indeed, it has been shown that
304 C-proteinase activity is sensitive to inhibitors of *N*-glycosylation (Duksin et al., 1978). Loss of giantin
305 function affects the enzyme composition of the Golgi and the *O*-glycosylation of specific substrates (Lan et
306 al., 2016; Stevenson et al., 2017). It is thus feasible that at least one of the N-propeptidases is incorrectly
307 glycosylated in giantin KO cells in such a way as to impede activity. Alternatively, procollagen itself may be
308 incorrectly glycosylated preventing its identification as a substrate. We did perform a global analysis of
309 glycoproteins by mass spectrometry but, as predicted from previous results (Stevenson et al., 2017), there
310 were no differences in the major glycosyl chains produced by WT or KO cell lines. This approach did not
311 permit us to determine the glycosylation of specific substrates.

312 A crucial observation made in this study is that N-propeptide processing occurs, at least in part, inside the
313 cell since cleaved N-propeptide, but not C-propeptide, is readily detectable in the lysates of WT cells. Whilst
314 it is possible that this pool of N-propeptide is in fact extracellular N-propeptide associated with the cell
315 surface or ECM, we rule this out for several reasons. Firstly, care was taken to lyse the cells gently and leave
316 the ECM behind. Secondly, N-propeptide in the cell layer fraction was sensitive to inhibitors of both
317 lysosomal and proteasomal degradation. Thirdly, N-propeptides have been noted to have biological
318 functions consistent with intracellular localisation (Oganesian et al., 2006). Finally, there is precedent for
319 the detection of intracellular procollagen processing in both chick and mouse tendons (Canty-Laird et al.,
320 2012; Canty et al., 2004; Humphries et al., 2008). In these studies, processed forms of type I procollagen
321 were detected in a detergent soluble fraction from tendon explants, consistent with an intracellular pool.
322 Furthermore, inhibition of procollagen secretion by BFA treatment, which causes the cis- and medial-Golgi
323 machinery to accumulate in the ER, does not prevent N-terminal processing, indicating procollagen can be
324 processed in the early secretory pathway where giantin is located (Canty-Laird et al., 2012). Considering
325 this, together with the data presented here, we conclude that giantin is a crucial component of an
326 intracellular pathway of procollagen processing.

327 Classically, human patients with mutations affecting N-terminal processing of type I procollagen suffer from
328 Ehlers-Danlos syndrome (EDS) type VII, a disease characterised by joint hypermobility, skin
329 hyperextensibility, and dislocations (Byers et al., 1997; Colige et al., 1999; Giunta et al., 1999; Smith et al.,
330 1992). Collagen fibres in these patients tend to be thinner and have irregular contours (Malfait et al., 2013;
331 Van Damme et al., 2016). ADAMTS2 deficient mice also have thinner collagen fibrils in the skin (Li et al.,
332 2001). This is not what we observe in the CDM of *GOLGB1* KO cells and the characteristics of EDS patients
333 have not been described in *GOLGB1* KO animals or humans. There are several reasons why giantin loss may
334 not mimic an EDS phenotype. Firstly, prior RNAseq data shows that the expression of many matrix

335 components is altered following loss of giantin (Stevenson et al., 2017). We believe this may be
336 compensatory in both cells and zebrafish and must affect matrix quality more globally. Giantin also impacts
337 ciliary function which would compound phenotypes (Asante et al., 2013; Stevenson et al., 2017). Secondly,
338 we do not exclude the possibility that N-terminal processing still occurs in the extracellular space in our
339 systems. In fact, we think it likely given the mild impact on matrix organisation observed. In cases of EDS
340 type VII, mutations in ADAMTS2 or the N-terminus of pro-α1(I) directly impact N- propeptide cleavage
341 regardless of location or environmental conditions. We propose giantin acts more indirectly to regulate an
342 intracellular processing pathway which acts in concert with other complimentary mechanisms, such as
343 extracellular cleavage, for co-ordinated and efficient processing under different conditions. This raises the
344 intriguing possibility of specific pools of collagen that require intracellular processing for specific functions,
345 such as fracture repair.

346 We found that *COL1A1* gene expression is reduced in both *golgb1*$^{X3078/X3078}$ mutant zebrafish and KO cells
347 (Stevenson et al., 2017). This contrasts with protein levels which are more abundant *in vitro*, at least in the
348 cells we have analysed here. Previous studies have suggested that the pro-α1(I) N-propeptide is capable of
349 acting as a negative regulator of pro-α1(I) synthesis (Horlein et al., 1981; Oganesian et al., 2006; Paglia et
350 al., 1979; Wiestner et al., 1979). Importantly, the point of inhibition occurs during translational chain
351 elongation or termination (Horlein et al., 1981; Oganesian et al., 2006; Paglia et al., 1979). Thus, we
352 propose that despite the reduced abundance of mRNA transcript, translation of pro-α1(I) is more efficient
353 in giantin KO cells in the absence of inhibitory N-propeptide. Consistent with reports that only
354 endogenously expressed N-propeptide can inhibit translation, we were unable to rescue our phenotypes by
355 supplementing media with recombinant type I procollagen N-propeptide.

356 As previously described, *golgb1*$^{X3078/X3078}$ mutant zebrafish show developmental growth delay, elongated
357 craniofacial structures and ectopic mineralisation of soft tissue (Stevenson et al., 2017). Here, we
358 additionally report that mutant adult caudal fins accumulate significant numbers of fractures and show
359 defects in the maturation of newly deposited matrix during fracture repair. Our observations of increased
360 calcein labelling in mutant fish fractures is consistent with either increased osteoid formation or hyper-
361 mineralisation. We have previously reported that expression of the glycosyltransferase GALNT3 is reduced
362 in both *GOLGB1* KO cells and zebrafish (Stevenson et al., 2017). GALNT3 is required to glycosylate and
363 activate FGF23, which is an inhibitor of bone mineralisation (Wang et al., 2008). The observed defects in
364 fracture repair could therefore be the result of FGF23 deficiency.

365 Alternatively, or perhaps additionally, collagen N-propeptides have been linked to the differentiation and
366 apoptosis of osteoblasts (Oganesian et al., 2006) and osteoclasts (Hayashi et al., 2011) respectively. We
367 have not been able to directly demonstrate that the procollagen processing defects observed in cells
368 translate to fish, however it is interesting to speculate that processing defects may affect the balance of
369 bone synthesis and resorption in the mutant fractures. The significant impact of the loss of giantin on
370 mineralisation likely explains why mutant animals primarily present with skeletal defects and other type I
371 collagen rich tissues, such as skin, are less affected.

372 The observed increased incidence of fractures in mutants could result from an increased frequency of
373 fractures in brittle bones or an accumulation of fractures due to slow healing. Although fracture repair is
374 delayed in the mutants, our data show that the described differences between WT and mutant fractures
375 largely resolve within three weeks. This seems insufficient to account for number of spontaneous fractures
376 that accumulate, given that callouses can persist for months overall (Geurtzen et al., 2014). Combined with
377 the clustered nature of a significant number of fractures we believe it likely that the bones are more brittle.
378 This would be consistent with a defect in type I collagen deposition, as mutations in the *COL1A1* gene are
379 associated with osteogenesis imperfecta in both humans (Glorieux, 2008) and zebrafish (Fisher et al., 2003;
380 Gistelinck et al., 2018). Some N-propeptide processing deficiencies can cause disease with characteristics of
381 both osteogenesis imperfecta and EDS in humans (Cabral et al., 2005; Makareeva et al., 2006). Giantin KO
382 also affects the abundance of other matrix proteins affecting bone quality (Stevenson et al., 2017). Further
383 study will be needed to define which, if any, phenotypes seen in zebrafish are a direct result of defective N-
384 terminal processing of type I procollagen.

Acknowledgements

We would like to thank Franck Perez and Gaelle Boncompain (Institut Curie, France) for sharing the RUSH system with us, Helen Dawe (University of Exeter, UK) and Stuart Haslam (Imperial College London, UK) for their technical help and advice, Andrew Herman and the UoB flow cytometry facility for sorting our cell lines, Kate Heesom and the UoB proteomics facility for performing exploratory mass spec runs, Lucy McGowan for her assistance with the fish experiments, and Alain Colige (University of Liege, Belgium) for his help and advice and for providing an ADAMTS2 construct. This work was funded by the MRC (MR/P000177/1) and Versus Arthritis (21937 and 22044). We also thank the MRC and Wolfson Foundation for establishing the Wolfson Bioimaging Facility, and confocal microscopy was supported by a BBSRC ALERT 13 capital grant (BB/L014181/1). Thanks to Karl Kadler for critical reading of the manuscript. The authors declare no competing financial interests.

Author Contributions

Conceptualisation D.J.S & N.L.S. Formal analysis N.L.S. Funding acquisition and supervision D.J.S & C.L.H. Investigation and methodology N.L.S and D.J.M.B. Project administration D.J.S. Visualisation N.L.S. Writing original draft N.L.S and D.J.S. Writing review and editing NLS, D.J.M.B, D.J.S, and C.L.H.

402 **Supplemental Figures**

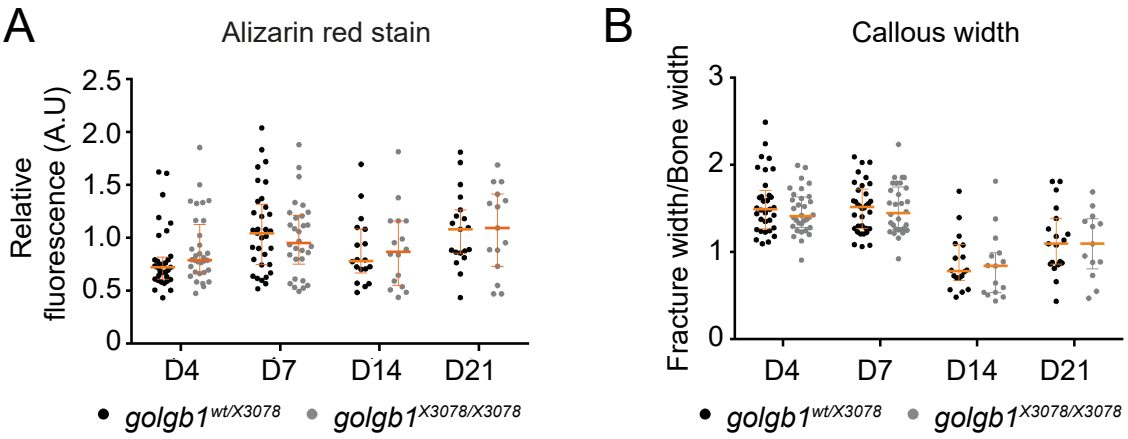

403

404 **Supplemental Figure 1. Fracture analysis in WT and mutant zebrafish. A-B.** Quantification of (A) the
405 intensity of alizarin red staining and (B) callous width of experimentally induced fractures normalised to
406 adjacent healthy bone at different timepoints post injury (D=days post injury) in *golgb1*$^{wt/X3078}$ and
407 *golgb1*$^{X3078/X3078}$ fish. Dots represent individual fractures. At timepoints 4 and 7 d.p.f eleven fish per line
408 were quantified. At timepoints 14 and 21 d.p.f n= 6 HETs and n=4 HOM fish. All from a single experiment.
409 Horizontal and vertical orange lines depict median and interquartile range respectively. P value calculated
410 with a Mann Whitney test comparing the mean value per fish (three fractures per fish).

411

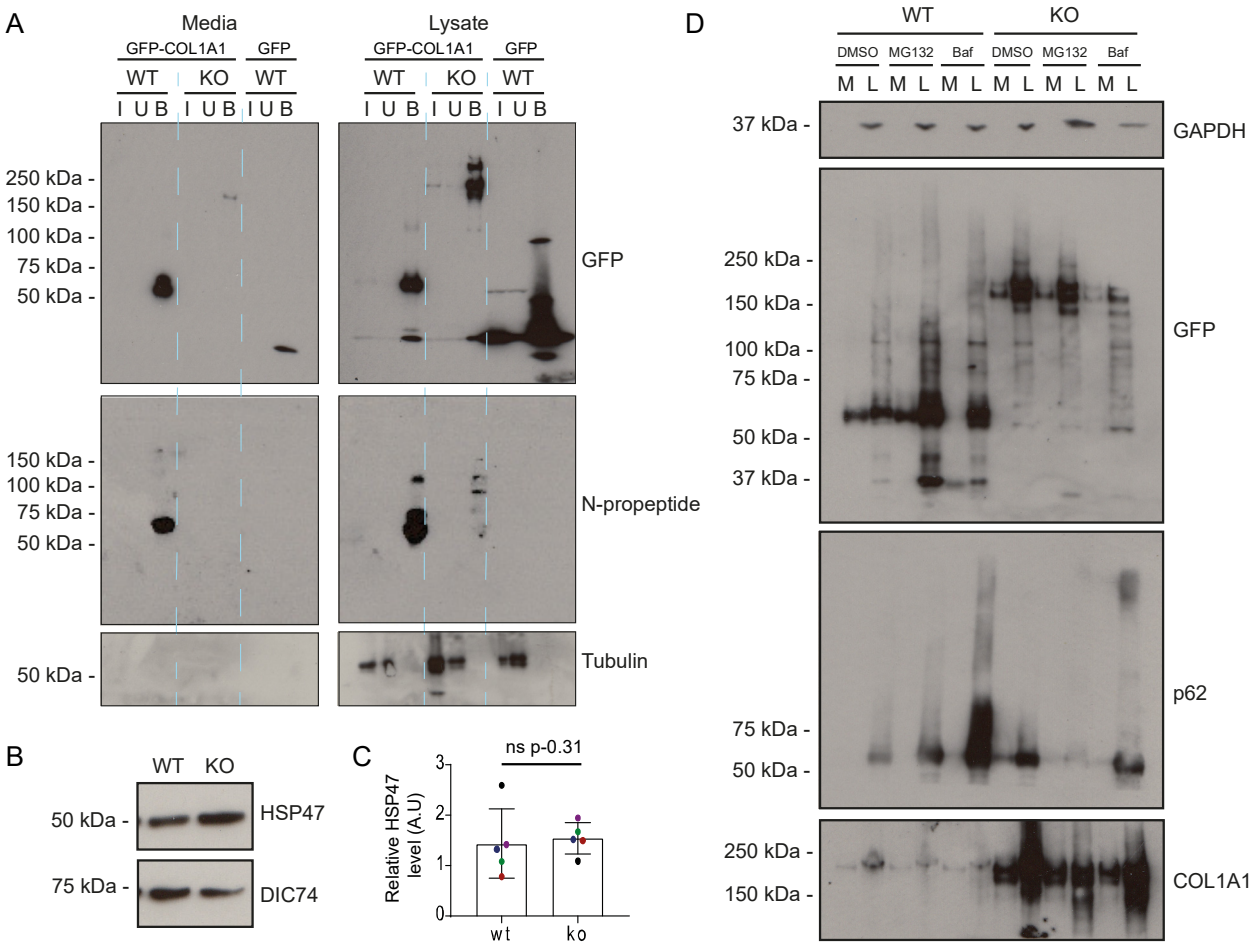

Supplemental Figure 2. Procollagen processing controls. A. Western blot of a GFP trap of media (M) and lysates (L) fractions of WT and KO cell cultures. Cells were either expressing GFP-COL1A1 or GFP alone as indicated. Blots show the input (I), unbound (U) and bound (B) fractions of the IP immunoblotted for GFP, type I procollagen N-propeptide (LF39 antibody), and tubulin (housekeeping). **B**. Western blot of HSP47 and DIC74 (housekeeping) in WT and giantin KO RPE1 cell lysates. **C.** Densitometry of the semi-quantitative ECL western blots represented in (A). HSP47 levels are normalised to DIC74. Each dot represents an independent biological replicate and replicates are colour coded between cell lines. Bars show median and interquartile range (n=5 biological replicates). P value calculated with a Mann Whitney test. **D.** Western blots of media (M) and lysate (L) fractions of WT and giantin KO cell cultures stably expressing GFP-COL1A1 following treatment with DMSO (vehicle control), MG132 or bafilomycin (baf). Blots are probed for GAPDH (housekeeping), GFP (GFP-COL1A1), p62 (positive control for bafilomycin) and pro-α1(I) (COL1A1) as indicated.

```
EXON 13

WT:
5'...AAGCTACAGGAAGCCTTAACCTCCCGCA AGGCAATTCTTAAAAAGGCACAGGAGAAAGAAAGACATCTCAGGGAGGAGCTAAAG...3'
N ... K  L  Q  E  A  L  T  S  R  K  A  I  L  K  K  A  Q  E  K  E  R  H  L  R  E  E  L  K...C

MUTANT 13_2
5'...AAGCTACAGGAAGCCTTAACCTCCC CGCAAGGCAATTCTTAAAAAGGCACAGGAGAAAGAAAGACATCTCAGGGAGGAGCTAAAG...3'
N ... K  L  Q  E  A  L  T  S   P  Q  G  N  S  *  ...C

5'...AAGCTACAGGAAGCCTTAACCTCC GCAAGGCAATTCTTAAAAAGGCACAGGAGAAAGAAAGACATCTCAGGGAGGAGCTAAAG...3'
N ... K  L  Q  E  A  L  T  S   A  R  Q  F  L  K  R  H  R  R  K  K  D  I  S  G  R  S  *  ...C

MUTANT 13_3
5'...AAGCTACAGGAAGCCTTAA A       AAGGCAATTCTTAAAAAGGCACAGGAGAAAGAAAGACATCTCAGGGAGGAGCTAAAG...3'
N ... K  L  Q  E  A  L  K          R  Q  F  L  K  R  H  R  R  K  K  D  I  S  G  R  S  *  ...C

MUTANT 13_4
5'...AAGCTACAGGAAGCCTTAACCTCC GCAAGGCAATTCTTAAAAAGGCACAGGAGAAAGAAAGACATCTCAGGGAGGAGCTAAAG...3'
N ... K  L  Q  E  A  L  T  S   A  R  Q  F  L  K  R  H  R  R  K  K  D  I  S  G  R  S  *  ...C
```

Supplemental figure 3. Validating pro-α1(I) processing defect in other giantin KO clones. Genomic DNA sequence and amino acid translation at CRISPR/Cas9 mutation site in three new giantin KO clones targeted at exon 13. On the WT sequence the gRNA sequence is indicated with a purple line, the cut site is indicated by scissors and PAM site is in blue text. In mutant sequences red text indicated inserted base pairs in genomic sequence and green text shows altered amino acids. Asterisks denote premature stop codons.

Legends to Supplemental Movies

Supplemental Movie 1

Representative movie of a RUSH assay in a WT RPE1 cell stably stably expressing GFP-COL1A1 (green) and transiently transfected with mCh-ST (magenta, Golgi label) and an ER RUSH hook. At time 0 biotin and ascorbic acid were added to the medium to release the collagen from the hook and promote procollagen folding respectively to trigger anterograde trafficking. Movie is cropped to the relevant time frame – time is indicated in top left corner as mm:ss. Frames were captures as single frame images every 20 seconds. Movie frame rate 12 frames/s. Scale bar 10 µm.

Supplemental Movie 2

Representative movie of a RUSH assay in a Giantin KO RPE1 cell stably expressing GFP-COL1A1 (green) and transiently transfected with mCh-ST (magenta, Golgi label) and an ER RUSH hook. At time 0 biotin and ascorbic acid were added to the medium to release the collagen from the hook and promote procollagen folding respectively to trigger anterograde trafficking. Movie is cropped to the relevant time frame – time is indicated in top left corner as mm:ss. Frames were captures as single frame images every 20 seconds. Movie frame rate 12 frames/s. Scale bar 10 µm.

451 # Methods

452 ## Zebrafish husbandry and genetic lines.

453 London AB zebrafish were maintained using standard conditions (Alestrom et al., 2019). Ethical approval
454 was obtained (University of Bristol Ethical Review Committee) and experiments performed under Home
455 Office Project License number 30/3804. The *golgb1*^{bsl077} (henceforth *golgb1*^{X3078}) allele is described in
456 (Stevenson et al., 2017). The *golgb1*^{X3078} allele was crossed with fish carrying the *Tg(col1a1a:EGFP)*^{zf195tg}
457 (henceforth *col1a1a:GFP*) transgenic reporter of the 1.4 kb *col1a1a* promoter region (Kague et al., 2012).
458 The GFP positive *golgb1*$^{wt/X3078}$ + *col1a1a:GFP* individuals were in-crossed to generate homozygotes. In all
459 experiments, homozygotes were compared to siblings.

460 ## Fin fracture assays

461 Fin fractures were performed as previously described (Geurtzen et al., 2014). Briefly, 7-month-old adult fish
462 were anaesthetised with MS222 (Sigma-Aldrich) and moved into a petri dish with the head placed on a bed
463 of tissue soaked in anaesthetic and the tail splayed on the dish for imaging. Caudal fins were imaged prior
464 to injury and any pre-existing fractures counted. Fractures were induced by pressing on an individual
465 segment of bone in the tail rays with the end of a semi-flexible plastic pipette tip. Four fractures per fish
466 were introduced in non-pigmented sections of fin in the distal third of the tail, avoiding the four most
467 dorsal and ventral rays. Fish were then reimaged live at various time points post-injury.

468 ## Live staining of bone

469 To visualise bone repair in live zebrafish, Alizarin Red stain (ARS) and calcein green stain was used. ARS
470 staining solution contained 74 µM Alizarin Powder (Sigma-Aldrich) and 5 mM HEPES dissolved in Danieau's
471 buffer. Calcein green staining solution contained 40 µM calcein powder (Sigma-Aldrich) dissolved in
472 Danieau's buffer and was pH calibrated to pH 7.4. Live fish were immersed in either ARS or calcein green
473 for two hours, then immersed in fresh system water for 15 minutes prior to imaging to clear excess stain
474 from the fish.

475 Fluorescence intensity at fracture sites was measured using image j – lines were drawn along the fracture
476 callous length and then the line width expanded to encompass the whole fracture. The mean intensity was
477 then measured across this area, before using the same ROI to measure the mean intensity of adjacent,
478 uninjured hemi-ray. Fracture intensity was then normalised against the healthy bone to account for
479 differences in baseline expression caused by reporter integration number.

480 ## Cell lines and culture

481 Human telomerase-immortalised retinal pigment epithelial cells (hTERT-RPE1, ATCC) were grown in DMEM-
482 F12 (Life Technologies, Paisley, UK) supplemented with 10% decomplemented FCS (Gibco). Cell lines were
483 not authenticated after purchase other than confirming the absence of mycoplasma contamination. The
484 main *GOLGB1* KO hTERT-RPE1 cell line used is described in (Stevenson et al., 2017).

485 New *GOLGB1* KO cell lines with mutations in exon 13 were generated using the lentiCRISPRv2 system
486 (lentiCRISPR v2 was a gift from Feng Zhang (Addgene plasmid # 52961; http://n2t.net/addgene:52961;
487 RRID: Addgene 52961)). Guide RNA sequences were designed using Benchling (http://benchling.com) and
488 inserted into the lentiCRISPRv2 construct as described in (Sanjana et al., 2014; Shalem et al., 2014) to be co-
489 expressed with Cas9. [Target sequences used: 5' - CCACCGGGAAGCCTTAACCTCCCGCA - 3' and 5' --
490 AAACTGCGGGAGGTTAAGGCTTCCC – 3']. The cloned plasmid was packaged into lentivirus using lenti-X-
491 packaging-single-shots (VSVG) (Takara, #631275) according to the manufacturer's instructions. After
492 harvest, 1 ml virus supernatant was added to 80% confluent RPE1 cells in a 6cm dish (after removal of
493 growth media) in the presence of 8 µg/ml polybrene. Virus was incubated for 1 h before adding back fresh
494 growth medium supplemented with 8 µg/ml polybrene. Transfection medium was replaced after 24 h. Cells
495 were passaged 24 h later in 20 µg/ml puromycin to select transfected cells. After seven days, individual
496 cells were FACS sorted into a 96 well plate to grow up clones and screen for *GOLGB1* knockout by
497 immunofluorescence and western blot. To identify the mutations, genomic DNA was extracted from each

498 clone using the Purelink genomic DNA mini kit (Invitrogen) and the region targeted by the gRNAs was
499 amplified by PCR [primers: forward 5' - GCTGGCAGCTGAAGAGCAATTCCA - 3' reverse 5' -
500 GTTGAGTGTGATGCTGTTCTGTGGCT - 3']. PCR products were cloned into the pGEM-T Easy vector according
501 to the manufacturer's instructions (Promega) and sequenced using predesigned primers against the T7
502 promoter (MWG Eurofins).

503 Stable cell lines were made by lentiviral transduction as described above using the Lenti-X Single shot
504 lentivirus packaging system (Takara, #631275) in combination with the lentiviral vector pLVXpuro-proSBP-
505 GFP-COL1A1 (Addgene #110726) described in (McCaughey et al., 2019). To ensure only low levels of over-
506 expression all cell lines were FACs sorted. GFP only stable cells are described in (Asante et al., 2014).

507 Transient transfections were performed using Lipofectamine 2000 according to the manufacturer's
508 instructions using 2 µg DNA for a 35 mm well (Invitrogen, Carlsbad, CA, Cat# 11668027). Plasmid: Str-KDEL-
509 IRES-ST-mCherry is described in (McCaughey et al., 2019) (Addgene; no. 110727).

510 **Antibodies**

511 Rabbit anti-COL1A1 (Novus Cat# NB600-408, RRID:AB_10000511), mouse anti-DIC74 (Millipore Cat#
512 MAB1618, RRID:AB_2246059), mouse anti-HSP47 (Enzo Life Sciences Cat# ADI-SPA-470,
513 RRID:AB_10618557), mouse anti-GM130 (BD Biosciences Cat# 610823, RRID:AB_398142), rabbit anti-
514 giantin (N-terminus, BioLegend Cat# 924302, RRID:AB_2565451), rabbit anti-giantin (C-terminus, gift from
515 Martin Lowe), mouse anti-SBP clone 20 (Millipore Cat# MAB10764, RRID:AB_10631872), rabbit polyclonal
516 anti–N- and C-propeptide of COL1A1 (LF-39 and LF-41 respectively, both gifts from Larry Fisher, National
517 Institutes of Health, Bethesda, MD;(Fisher et al., 1995)), mouse monoclonal anti-GFP (Covance Cat# MMS-
518 118P-500, RRID:AB_291290), sheep polyclonal anti-GRASP65 (gift from Jon Lane), tubulin (Sigma-Aldrich
519 Cat# T5168, RRID:AB_477579), mouse monoclonal anti-Sec31A (BD Biosciences Cat# 612350,
520 RRID:AB_399716), mouse p62 (Novus Cat# H00008878-D01P, RRID:AB_1504204). Secondary HRP-
521 conjugated antibodies were obtained from Jackson ImmunoResearch. Alexa-Fluor® conjugated secondaries
522 were obtained from Invitrogen.

523 **Immunofluorescence**

524 Cells were grown on autoclaved coverslips (0.17 mm thickness #1.5 Thermo Fisher Scientific) prior to
525 fixation with 4% PFA/PBS for 10 minutes, permeablilsation with 1% Triton X-100/PBS for 10 minutes and
526 blocking with 3% BSA/PBS for 30 minutes. Sequential incubations with primary and secondary antibodies
527 diluted in block were performed for one hour, washing in PBS in between. Nuclei were labelled with DAPI
528 (4,6-diamidino-2-phenylindole; Life Technologies, D1306) for 3 minutes. Coverslips were mounted in
529 MOWIOL 4-88 (Merck-Millipore). All steps were conducted at room temperature and in the dark post-
530 secondary antibody addition. When labelling for extracellular matrix, the triton permeability step was
531 excluded from the protocol.

532 For widefield microscopy an Olympus IX-71 inverted microscope was used with a 60×1.42 NA oil-immersion
533 lens, Exfo Excite xenon lamp illumination, and single-pass excitation, emission and multipass dichroic
534 (Semrock) filters. Images were captured on an Orca-ER CCD (Hamamatsu). The system was controlled using
535 Volocity (v.5.4.1; PerkinElmer). Chromatic shifts in images were registration corrected using TetraSpek
536 fluorescent beads (Thermo Fisher Scientific). Fixed cell imaging by confocal microscopy was performed
537 using a Leica SP5II system at 1024x1024 xy resolution. Tilescans were performed to capture larger areas of
538 the CDM. On both systems, image stacks were taken with Δz of 0.2 µm and, unless indicated, maximum
539 projections are shown. Image processing was performed using ImageJ software (Schindelin et al., 2012).

540 **Preparation of the cell derived matrix**

541 To prepare the cell derived matrix, cells were grown for 3 days on coverslips until they reached confluence
542 and then 50 ug/ml L-ascorbic acid-2-phosphate (Sigma Aldrich) was added to cultures. Cells were left for a
543 further seven days. To prepare samples, cells were washed in PBS and extracted using pre-warmed
544 extraction buffer (20 mM NH_4OH, 0.5% Triton X-100 in PBS; 3 ml per 6 cm plate for 2 minutes). After three
545 water washes, residual DNA was digested with 10 ug/ml DNase I (Roche) for 30 min at 37°C and then

546 extracts were washed again. For immunofluorescence experiments, the matrix was fixed in 4% PFA and
547 stained as above. For scanning electron microscopy, extracts were fixed with 2% PFA, 2.5% glutaraldehyde
548 in 0.1M cacodylate buffer for 2 hours at room temperature. All coverslips were then washed 2x with 0.1M
549 cacodylate buffer before undergoing progressive dehydration with 70, 80, 90, 96, 100, 100% EtOH for 15
550 minutes each. They were left in 100% ETOH for 1 h before drying in a critical point drier (50% spin, 120s
551 delay between cycles, 15 CO_2 cycles (13C cool, 15 cycles, 35C heat), speed 5). Samples were then sputter
552 coated (40mA and 30 seconds). Coverslips were imaged on a FEI Quanta 200 FEG-SEM microscope.

553 **Live imaging**

554 Procollagen trafficking was analysed using the retention using selective hooks (RUSH) assay (Boncompain et
555 al., 2012). Cells stably expressing pro-SBP-GFP-COL1A1 were grown on 35 mm MatTek glass-bottomed
556 dishes (MatTek) and transfected with Str-KDEL-IRES-ST-mCherry (McCaughey et al., 2019) 24 hours prior to
557 imaging. Cells were always confluent at time of imaging.

558 To image, growth media was replaced with 1 ml prewarmed Fluorobrite DMEM (Thermo-Fisher, A1896701)
559 and the dishes mounted on a Leica SP8 confocal laser scanning microscope system with a 63x HC OL APO
560 CS2 1.42 numerical aperture glycerol lens and an environmental chamber at 37°C with CO_2 enrichment. The
561 microscope was controlled with Leica LAS X software. Once GFP- and mCh-positive cells were identified, 1
562 ml Fluorobrite containing 800 µM biotin and 1000 µg/ml L-ascorbic acid-2-phosphate (Sigma Aldrich,
563 A92902) was added to the dish (final concentration 400 µM biotin and 500 µg/ml respectively) to induce
564 procollagen folding and synchronous release of the pro-SBP-GFP-COL1A1 from the ER hook. This is T = 0.
565 Cells were then imaged live, taking a single confocal plane image every 20 seconds. Fluorophores were
566 excited using a 65-mW Argon and 20-mW solid state yellow lasers and detected using hybrid GaAsP
567 detectors. Imaging conditions for movies: 1024x1024 pixel resolution, scanning speed 600 Hz, 2x zoom, 3-
568 line average, imaging sequentially between frames. Fluorophores were excited using a 65-mW Argon laser
569 at 488 nm and a 20-mW solid state yellow laser at 561 nm and detected using hybrid GaAsP detectors and
570 corresponding notch filters.

571 To immediately fix during live imaging, 2 ml 8% PFA was added to the 2 ml Fluorobrite already present at
572 the desired time point. Cells were fixed for 10 minutes and the above immunofluorescence protocol
573 applied.

574 **Secretion assays, IPs and immunoblotting**

575 To perform secretion assays, media was aspirated from confluent cells and replaced with a minimal volume
576 of serum free DMEM-F12 supplemented with 50 µg/ul L-ascorbic acid-2-phosphate (Sigma Aldrich,
577 A92902). Cells were left overnight at 37°C and 5% CO_2. Media was then collected and the cell layer was
578 rinsed with PBS, lysed in RIPA buffer (50 mM Tris-HCl, pH 7.5, 300 mM NaCl, 2% Triton X-100, 1%
579 deoxycholate, 0.1% SDS, 1 mM EDTA) for 30 minutes rocking on ice, and collected without scraping. Media
580 and lysate fractions were spun at 13000 x g at 4°C for 10 minutes and the supernatants used for SDS-PAGE.
581 For collection of lysates in other experiments, cells were scraped in RIPA buffer, collected in tubes and
582 incubated on a rotator at 4°C for 30 minutes. BCA assays were performed where necessary to determine
583 protein concentration according to the manufacturer's instructions (BioRad). Samples were boiled in 1x LDS
584 sample buffer (Life Technologies, NP007) containing sample reducing agent (Life Technologies, NP007) for
585 10 minutes at 95°C.

586 For inhibitor experiments, confluent cells were treated with 1 ml serum free medium containing either
587 DMSO (control), 10 µM MG132 or 200 nM bafilomycin overnight before media and lysate collection.

588 For GFP-trap® immunoprecipitation, confluent cells were serum starved for 24 h in the presence of 50 µg/ul
589 L-ascorbic acid-2-phosphate (Sigma Aldrich, A92902). At the time of assay, media was collected and spun at
590 2700 x g for 5 minutes to remove dead cells. The cell layer was washed twice with ice-cold PBS and lysed in
591 ice cold buffer (10 mM Tris-HCl pH 7.4, 50 mM NaCl, 0.5 mM EDTA, 1.0% Igepal CA-630, 1 mM PMSF and 1x
592 Protease inhibitor cocktail (Millipore, 539137)) for 30 minutes with agitation on a rotator. Lysate
593 supernatant was collected by centrifuging at 20 000 x g for 10 minutes and 66 µl was removed to be used

594 as an 'input' reference sample. Media and lysate supernatants were then incubated with equilibrated GFP
595 nano-trap beads (Chromotek) on a rotator for two hours. Beads were pelleted by centrifugation at 2000 x g
596 for 2 minutes. The supernatant was removed but 66 µl kept as an 'unbound' reference sample. The beads
597 were then washed three times with 500 µl dilution buffer (10 mM Tris-HCl pH 7.4, 50 mM NaCl, 0.5 mM
598 EDTA, 1 mM PMSF and 1x Protease inhibitor cocktail), pelleting them each time by centrifugation at 2000 x
599 g for 2 minutes. All steps to this point were carried out on ice/at 4°C. Finally, beads were resuspended in 88
600 µl 1x LDS sample buffer (Life Technologies, NP007) containing sample reducing agent (Life Technologies)
601 Inbound and unbound samples were mixed with 22 µl 4x LDS sample buffer + reducing agent (Life
602 Technologies). Samples were boiled at 95 ^{o}C for 10 mins.

603 Secretion assays, IP and lysate samples were separated by SDS-PAGE on precast 3-8% tris-acetate and 4-
604 12% bis-tris acrylamide gels (Invitrogen) followed by transfer to 0.2 µm nitrocellulose membranes
605 (Amersham). Membranes were blocked in 5% milk 0.05% Tween (Sigma) in tris buffered saline for at least
606 1h. Primary and HRP-conjugated secondary antibodies were diluted in block and sequentially incubated
607 with the membrane for 2-16 h each. HRP was detected by enhanced chemiluminescence (Promega ECL, GE
608 healthcare film).

609 **Statistical analyses**

610 Measurements of images and western blots were carried out using Image J. Statistical analyses were
611 performed using GraphPad Prism 7.00. The tests used, n numbers and sample sizes are indicated in the
612 figure legends, P-values where significant ($p<0.05$) are shown on the figures. All experiments were analysed
613 with non-parametric tests as data was not normally distributed. Sample sizes were chosen based on
614 previous, similar experimental outcomes and based on standard assumptions. No samples were excluded.

615

616 **References**

617 Alestrom, P., L. D'Angelo, P.J. Midtlyng, D.F. Schorderet, S. Schulte-Merker, F. Sohm, and S. Warner. 2019.
618 Zebrafish: Housing and husbandry recommendations. *Lab Anim*:23677219869037.
619 Asante, D., L. Maccarthy-Morrogh, A.K. Townley, M.A. Weiss, K. Katayama, K.J. Palmer, H. Suzuki, C.J.
620 Westlake, and D.J. Stephens. 2013. A role for the Golgi matrix protein giantin in ciliogenesis
621 through control of the localization of dynein-2. *J Cell Sci*. 126:5189-5197.
622 Asante, D., N.L. Stevenson, and D.J. Stephens. 2014. Subunit composition of the human cytoplasmic dynein-
623 2 complex. *J Cell Sci*. 127:4774-4787.
624 Bekhouche, M., and A. Colige. 2015. The procollagen N-proteinases ADAMTS2, 3 and 14 in pathophysiology.
625 *Matrix Biol*. 44-46:46-53.
626 Bergen, D.J.M., N.L. Stevenson, R.E.H. Skinner, D.J. Stephens, and C.L. Hammond. 2017. The Golgi matrix
627 protein giantin is required for normal cilia function in zebrafish. *Biol Open*. 6:1180-1189.
628 Bergen, D.J.M., E. Kague, and C.L. Hammond. 2019. Zebrafish as an Emerging Model for Osteoporosis: A
629 Primary Testing Platform for Screening New Osteo-Active Compounds. *Front Endocrinol (Lausanne)*.
630 10:6.
631 Boncompain, G., S. Divoux, N. Gareil, H. de Forges, A. Lescure, L. Latreche, V. Mercanti, F. Jollivet, G.
632 Raposo, and F. Perez. 2012. Synchronization of secretory protein traffic in populations of cells. *Nat*
633 *Methods*. 9:493-498.
634 Bornstein, P., V. Walsh, J. Tullis, E. Stainbrook, J.F. Bateman, and S.G. Hormuzdi. 2002. The globular domain
635 of the proalpha 1(I) N-propeptide is not required for secretion, processing by procollagen N-
636 proteinase, or fibrillogenesis of type I collagen in mice. *J Biol Chem*. 277:2605-2613.
637 Broder, C., P. Arnold, S. Vadon-Le Goff, M.A. Konerding, K. Bahr, S. Muller, C.M. Overall, J.S. Bond, T.
638 Koudelka, A. Tholey, D.J. Hulmes, C. Moali, and C. Becker-Pauly. 2013. Metalloproteases meprin
639 alpha and meprin beta are C- and N-procollagen proteinases important for collagen assembly and
640 tensile strength. *Proc Natl Acad Sci U S A*. 110:14219-14224.
641 Byers, P.H., M. Duvic, M. Atkinson, M. Robinow, L.T. Smith, S.M. Krane, M.T. Greally, M. Ludman, R.
642 Matalon, S. Pauker, D. Quanbeck, and U. Schwarze. 1997. Ehlers-Danlos syndrome type VIIA and
643 VIIB result from splice-junction mutations or genomic deletions that involve exon 6 in the COL1A1
644 and COL1A2 genes of type I collagen. *Am J Med Genet*. 72:94-105.
645 Cabral, W.A., E. Makareeva, A. Colige, A.D. Letocha, J.M. Ty, H.N. Yeowell, G. Pals, S. Leikin, and J.C. Marini.
646 2005. Mutations near amino end of alpha1(I) collagen cause combined osteogenesis
647 imperfecta/Ehlers-Danlos syndrome by interference with N-propeptide processing. *J Biol Chem*.
648 280:19259-19269.
649 Canty-Laird, E.G., Y. Lu, and K.E. Kadler. 2012. Stepwise proteolytic activation of type I procollagen to
650 collagen within the secretory pathway of tendon fibroblasts in situ. *Biochem J*. 441:707-717.
651 Canty, E.G., and K.E. Kadler. 2005. Procollagen trafficking, processing and fibrillogenesis. *J Cell Sci*.
652 118:1341-1353.
653 Canty, E.G., Y. Lu, R.S. Meadows, M.K. Shaw, D.F. Holmes, and K.E. Kadler. 2004. Coalignment of plasma
654 membrane channels and protrusions (fibripositors) specifies the parallelism of tendon. *J Cell Biol*.
655 165:553-563.
656 Colige, A., S.W. Li, A.L. Sieron, B.V. Nusgens, D.J. Prockop, and C.M. Lapiere. 1997. cDNA cloning and
657 expression of bovine procollagen I N-proteinase: a new member of the superfamily of zinc-
658 metalloproteinases with binding sites for cells and other matrix components. *Proc Natl Acad Sci U S*
659 *A*. 94:2374-2379.
660 Colige, A., A.L. Sieron, S.W. Li, U. Schwarze, E. Petty, W. Wertelecki, W. Wilcox, D. Krakow, D.H. Cohn, W.
661 Reardon, P.H. Byers, C.M. Lapiere, D.J. Prockop, and B.V. Nusgens. 1999. Human Ehlers-Danlos
662 syndrome type VII C and bovine dermatosparaxis are caused by mutations in the procollagen I N-
663 proteinase gene. *Am J Hum Genet*. 65:308-317.
664 Colige, A., I. Vandenberghe, M. Thiry, C.A. Lambert, J. Van Beeumen, S.W. Li, D.J. Prockop, C.M. Lapiere, and
665 B.V. Nusgens. 2002. Cloning and characterization of ADAMTS-14, a novel ADAMTS displaying high
666 homology with ADAMTS-2 and ADAMTS-3. *J Biol Chem*. 277:5756-5766.

667 Duksin, D., J.M. Davidson, and P. Bornstein. 1978. The role of glycosylation in the enzymatic conversion of
668 procollagen to collagen: studies using tunicamycin and concanavalin A. *Arch Biochem Biophys*.
669 185:326-332.
670 Fernandes, R.J., S. Hirohata, J.M. Engle, A. Colige, D.H. Cohn, D.R. Eyre, and S.S. Apte. 2001. Procollagen II
671 amino propeptide processing by ADAMTS-3. Insights on dermatosparaxis. *J Biol Chem*. 276:31502-
672 31509.
673 Fisher, L.W., J.T. Stubbs, 3rd, and M.F. Young. 1995. Antisera and cDNA probes to human and certain animal
674 model bone matrix noncollagenous proteins. *Acta Orthop Scand Suppl*. 266:61-65.
675 Fisher, S., P. Jagadeeswaran, and M.E. Halpern. 2003. Radiographic analysis of zebrafish skeletal defects.
676 *Dev Biol*. 264:64-76.
677 Geurtzen, K., F. Knopf, D. Wehner, L.F. Huitema, S. Schulte-Merker, and G. Weidinger. 2014. Mature
678 osteoblasts dedifferentiate in response to traumatic bone injury in the zebrafish fin and skull.
679 *Development*. 141:2225-2234.
680 Gistelinck, C., R.Y. Kwon, F. Malfait, S. Symoens, M.P. Harris, K. Henke, M.B. Hawkins, S. Fisher, P. Sips, B.
681 Guillemyn, J.W. Bek, P. Vermassen, H. De Saffel, P.E. Witten, M. Weis, A. De Paepe, D.R. Eyre, A.
682 Willaert, and P.J. Coucke. 2018. Zebrafish type I collagen mutants faithfully recapitulate human
683 type I collagenopathies. *Proc Natl Acad Sci U S A*. 115:E8037-E8046.
684 Giunta, C., A. Superti-Furga, S. Spranger, W.G. Cole, and B. Steinmann. 1999. Ehlers-Danlos syndrome type
685 VII: clinical features and molecular defects. *J Bone Joint Surg Am*. 81:225-238.
686 Glorieux, F.H. 2008. Osteogenesis imperfecta. *Best Pract Res Clin Rheumatol*. 22:85-100.
687 Hayashi, S., Z. Wang, J. Bryan, C. Kobayashi, R. Faccio, and L.J. Sandell. 2011. The type II collagen N-
688 propeptide, PIIBNP, inhibits cell survival and bone resorption of osteoclasts via integrin-mediated
689 signaling. *Bone*. 49:644-652.
690 Horlein, D., J. McPherson, S.H. Goh, and P. Bornstein. 1981. Regulation of protein synthesis: translational
691 control by procollagen-derived fragments. *Proc Natl Acad Sci U S A*. 78:6163-6167.
692 Hulmes, D.J., K.E. Kadler, A.P. Mould, Y. Hojima, D.F. Holmes, C. Cummings, J.A. Chapman, and D.J. Prockop.
693 1989. Pleomorphism in type I collagen fibrils produced by persistence of the procollagen N-
694 propeptide. *J Mol Biol*. 210:337-345.
695 Humphries, S.M., Y. Lu, E.G. Canty, and K.E. Kadler. 2008. Active negative control of collagen fibrillogenesis
696 in vivo. Intracellular cleavage of the type I procollagen propeptides in tendon fibroblasts without
697 intracellular fibrils. *J Biol Chem*. 283:12129-12135.
698 Ishida, Y., H. Kubota, A. Yamamoto, A. Kitamura, H.P. Bachinger, and K. Nagata. 2006. Type I collagen in
699 Hsp47-null cells is aggregated in endoplasmic reticulum and deficient in N-propeptide processing
700 and fibrillogenesis. *Mol Biol Cell*. 17:2346-2355.
701 Kadler, K.E., Y. Hojima, and D.J. Prockop. 1987. Assembly of collagen fibrils de novo by cleavage of the type I
702 pC-collagen with procollagen C-proteinase. Assay of critical concentration demonstrates that
703 collagen self-assembly is a classical example of an entropy-driven process. *J Biol Chem*. 262:15696-
704 15701.
705 Kadler, K.E., D.J. Hulmes, Y. Hojima, and D.J. Prockop. 1990. Assembly of type I collagen fibrils de novo by
706 the specific enzymic cleavage of pC collagen. The fibrils formed at about 37 degrees C are similar in
707 diameter, roundness, and apparent flexibility to the collagen fibrils seen in connective tissue. *Ann N*
708 *Y Acad Sci*. 580:214-224.
709 Kague, E., M. Gallagher, S. Burke, M. Parsons, T. Franz-Odendaal, and S. Fisher. 2012. Skeletogenic fate of
710 zebrafish cranial and trunk neural crest. *PLoS One*. 7:e47394.
711 Katayama, K., M. Kuriki, T. Kamiya, Y. Tochigi, and H. Suzuki. 2018. Giantin is required for coordinated
712 production of aggrecan, link protein and type XI collagen during chondrogenesis. *Biochem Biophys*
713 *Res Commun*. 499:459-465.
714 Katayama, K., T. Sasaki, S. Goto, K. Ogasawara, H. Maru, K. Suzuki, and H. Suzuki. 2011. Insertional mutation
715 in the Golgb1 gene is associated with osteochondrodysplasia and systemic edema in the OCD rat.
716 *Bone*. 49:1027-1036.
717 Kessler, E., K. Takahara, L. Biniaminov, M. Brusel, and D.S. Greenspan. 1996. Bone morphogenetic protein-
718 1: the type I procollagen C-proteinase. *Science*. 271:360-362.

719 Kikukawa, K., T. Kamei, K. Suzuki, and K. Maita. 1990. Electron microscopic observations and
720 electrophoresis of the glycosaminoglycans in the epiphyseal cartilage of the congenital
721 osteochondrodysplasia rat (ocd/ocd). *Matrix*. 10:378-387.
722 Kikukawa, K., and K. Suzuki. 1992. Histochemical and immunohistochemical distribution of
723 glycosaminoglycans, type II collagen, and fibronectin in developing fetal cartilage of congenital
724 osteochondrodysplasia rat (ocd/ocd). *Teratology*. 46:509-523.
725 Koreishi, M., T.J. Gniadek, S. Yu, J. Masuda, Y. Honjo, and A. Satoh. 2013. The golgin tether giantin regulates
726 the secretory pathway by controlling stack organization within Golgi apparatus. *PLoS One*.
727 8:e59821.
728 Lan, Y., N. Zhang, H. Liu, J. Xu, and R. Jiang. 2016. Golgb1 regulates protein glycosylation and is crucial for
729 mammalian palate development. *Development*. 143:2344-2355.
730 Li, S.W., M. Arita, A. Fertala, Y. Bao, G.C. Kopen, T.K. Langsjo, M.M. Hyttinen, H.J. Helminen, and D.J.
731 Prockop. 2001. Transgenic mice with inactive alleles for procollagen N-proteinase (ADAMTS-2)
732 develop fragile skin and male sterility. *Biochem J*. 355:271-278.
733 Linstedt, A.D., and H.P. Hauri. 1993. Giantin, a novel conserved Golgi membrane protein containing a
734 cytoplasmic domain of at least 350 kDa. *Mol Biol Cell*. 4:679-693.
735 Makareeva, E., W.A. Cabral, J.C. Marini, and S. Leikin. 2006. Molecular mechanism of alpha 1(I)-
736 osteogenesis imperfecta/Ehlers-Danlos syndrome: unfolding of an N-anchor domain at the N-
737 terminal end of the type I collagen triple helix. *J Biol Chem*. 281:6463-6470.
738 Malfait, F., S. Symoens, N. Goemans, Y. Gyftodimou, E. Holmberg, V. Lopez-Gonzalez, G. Mortier, S.
739 Nampoothiri, M.B. Petersen, and A. De Paepe. 2013. Helical mutations in type I collagen that affect
740 the processing of the amino-propeptide result in an Osteogenesis Imperfecta/Ehlers-Danlos
741 Syndrome overlap syndrome. *Orphanet J Rare Dis*. 8:78.
742 McCaughey, J., N.L. Stevenson, S. Cross, and D.J. Stephens. 2019. ER-to-Golgi trafficking of procollagen in
743 the absence of large carriers. *J Cell Biol*. 218:929-948.
744 Michigami, T. 2019. Skeletal mineralization: mechanisms and diseases. *Ann Pediatr Endocrinol Metab*.
745 24:213-219.
746 Miyahara, M., K. Hayashi, J. Berger, K. Tanzawa, F.K. Njieha, R.L. Trelstad, and D.J. Prockop. 1984. Formation
747 of collagen fibrils by enzymic cleavage of precursors of type I collagen in vitro. *J Biol Chem*.
748 259:9891-9898.
749 Miyahara, M., F.K. Njieha, and D.J. Prockop. 1982. Formation of collagen fibrils in vitro by cleavage of
750 procollagen with procollagen proteinases. *J Biol Chem*. 257:8442-8448.
751 Munro, S. 2011. The golgin coiled-coil proteins of the Golgi apparatus. *Cold Spring Harb Perspect Biol*. 3.
752 Oganesian, A., S. Au, J.A. Horst, L.C. Holzhausen, A.J. Macy, J.M. Pace, and P. Bornstein. 2006. The NH2-
753 terminal propeptide of type I procollagen acts intracellularly to modulate cell function. *J Biol Chem*.
754 281:38507-38518.
755 Paglia, L., J. Wilczek, L.D. de Leon, G.R. Martin, D. Horlein, and P. Muller. 1979. Inhibition of procollagen
756 cell-free synthesis by amino-terminal extension peptides. *Biochemistry*. 18:5030-5034.
757 Petrosyan, A., M.S. Holzapfel, D.E. Muirhead, and P.W. Cheng. 2014. Restoration of compact Golgi
758 morphology in advanced prostate cancer enhances susceptibility to galectin-1-induced apoptosis by
759 modifying mucin O-glycan synthesis. *Mol Cancer Res*. 12:1704-1716.
760 Puthenveedu, M.A., and A.D. Linstedt. 2001. Evidence that Golgi structure depends on a p115 activity that
761 is independent of the vesicle tether components giantin and GM130. *J Cell Biol*. 155:227-238.
762 Romanic, A.M., E. Adachi, Y. Hojima, J. Engel, and D.J. Prockop. 1992. Polymerization of pNcollagen I and
763 copolymerization of pNcollagen I with collagen I. A kinetic, thermodynamic, and morphologic study.
764 *J Biol Chem*. 267:22265-22271.
765 Sanjana, N.E., O. Shalem, and F. Zhang. 2014. Improved vectors and genome-wide libraries for CRISPR
766 screening. *Nat Methods*. 11:783-784.
767 Satoh, A., M. Hayashi-Nishino, T. Shakuno, J. Masuda, M. Koreishi, R. Murakami, Y. Nakamura, T. Nakamura,
768 N. Abe-Kanoh, Y. Honjo, J. Malsam, S. Yu, and K. Nishino. 2019. The Golgin Protein Giantin
769 Regulates Interconnections Between Golgi Stacks. *Front Cell Dev Biol*. 7:160.

770 Schindelin, J., I. Arganda-Carreras, E. Frise, V. Kaynig, M. Longair, T. Pietzsch, S. Preibisch, C. Rueden, S.
771 Saalfeld, B. Schmid, J.Y. Tinevez, D.J. White, V. Hartenstein, K. Eliceiri, P. Tomancak, and A. Cardona.
772 2012. Fiji: an open-source platform for biological-image analysis. *Nat Methods*. 9:676-682.
773 Seelig, H.P., P. Schranz, H. Schroter, C. Wiemann, G. Griffiths, and M. Renz. 1994. Molecular genetic
774 analyses of a 376-kilodalton Golgi complex membrane protein (giantin). *Mol Cell Biol*. 14:2564-
775 2576.
776 Shalem, O., N.E. Sanjana, E. Hartenian, X. Shi, D.A. Scott, T. Mikkelson, D. Heckl, B.L. Ebert, D.E. Root, J.G.
777 Doench, and F. Zhang. 2014. Genome-scale CRISPR-Cas9 knockout screening in human cells.
778 *Science*. 343:84-87.
779 Smith, L.T., W. Wertelecki, L.M. Milstone, E.M. Petty, M.R. Seashore, I.M. Braverman, T.G. Jenkins, and P.H.
780 Byers. 1992. Human dermatosparaxis: a form of Ehlers-Danlos syndrome that results from failure to
781 remove the amino-terminal propeptide of type I procollagen. *Am J Hum Genet*. 51:235-244.
782 Stevenson, N.L., D.J.M. Bergen, R.E.H. Skinner, E. Kague, E. Martin-Silverstone, K.A. Robson Brown, C.L.
783 Hammond, and D.J. Stephens. 2017. Giantin-knockout models reveal a feedback loop between
784 Golgi function and glycosyltransferase expression. *J Cell Sci*. 130:4132-4143.
785 Tomecka, M.J., L.P. Ethiraj, L.M. Sanchez, H.H. Roehl, and T.J. Carney. 2019. Clinical pathologies of bone
786 fracture modelled in zebrafish. *Dis Model Mech*. 12.
787 Van Damme, T., A. Colige, D. Syx, C. Giunta, U. Lindert, M. Rohrbach, O. Aryani, Y. Alanay, P.O. Simsek-
788 Kiper, H.Y. Kroes, K. Devriendt, M. Thiry, S. Symoens, A. De Paepe, and F. Malfait. 2016. Expanding
789 the clinical and mutational spectrum of the Ehlers-Danlos syndrome, dermatosparaxis type. *Genet*
790 *Med*. 18:882-891.
791 Wang, H., Y. Yoshiko, R. Yamamoto, T. Minamizaki, K. Kozai, K. Tanne, J.E. Aubin, and N. Maeda. 2008.
792 Overexpression of fibroblast growth factor 23 suppresses osteoblast differentiation and matrix
793 mineralization in vitro. *J Bone Miner Res*. 23:939-948.
794 Wiestner, M., T. Krieg, D. Horlein, R.W. Glanville, P. Fietzek, and P.K. Muller. 1979. Inhibiting effect of
795 procollagen peptides on collagen biosynthesis in fibroblast cultures. *J Biol Chem*. 254:7016-7023.
796 Wong, M., and S. Munro. 2014. Membrane trafficking. The specificity of vesicle traffic to the Golgi is
797 encoded in the golgin coiled-coil proteins. *Science*. 346:1256898.

798